

Phase coexistence in a half-filled extended Hubbard model

Loïc Philoxene, Vu Hung Dao and Raymond Frésard

Normandie Université, ENSICAEN, UNICAEN, CNRS, CRISMAT, 14000 Caen, France

November 8, 2023

Abstract

In this Letter we analyze the coexisting ordered phases that arise in the half-filled ε - t - U - V extended Hubbard Model on the square lattice when tackled within the Kotliar and Ruckenstein slave boson representation in the thermodynamical limit. Particular emphasis is put on the dependence of the quasiparticle dispersions, the gaps, the spin-resolved renormalization factors, and the distribution of double occupancy on the microscopical parameters of the model. Our calculations are performed in a parameter range that is most suitable for resistive switching. In particular, the main contributions to the gaps are shown to either arise from ε in the weak coupling regime, or from U and V when they are the largest scales. The gaps are thus from joint spin and charge origin, and so are the order parameters.

1 Introduction

Stripe order made of magnetic moments and charges belongs to the hallmarks of doped layered Mott insulators. The modulated electronic phases consist of two-dimensional antiferromagnetic domains separated by hole-rich linear walls. Since their discovery in the superconducting Sr-doped La_2CuO_4 cuprates (LSCO)^{1,2}, they keep on being the subject of intense investigations^{3,4}. It would be fair to note, however, that they had already attracted a significant interest when they were first reported in doped nickelates^{5,6}. Furthermore, they have been evidenced in other families of transition-metal oxides as well, such as layered cobaltates⁷ and layered manganites⁸. Yet, not all stripy materials are alike. Indeed, the modulations are coined as diagonal or vertical, depending on the direction taken by their wave-vector in the Brillouin zone. Diagonal stripes are observed in all of these families of compounds, where they are found to be insulating^{9,10}. In contrast, vertical modulations are reported in cuprates, only, and they are associated with a metallic or, even, a superconducting state¹¹. For the latter group of oxides, model calculations have been able to establish a systematics of insulating diagonal filled and metallic half-filled stripes, with nearly one hole in the domain wall in the former case, and about half a hole in the latter case¹². But the interplay with d-wave superconductivity is more challenging to unravel. As a solution of the two-dimensional Hubbard model, stripe order has been found to be very close or lower in energy to its superconducting counterpart within a variety of numerical approaches¹³⁻¹⁹. Coexistence of both phases has been predicted, too^{20,21}, but not necessarily in the ground state²².

The origin of the stripe order can be qualitatively understood as follows for the Hubbard model on a square lattice with on-site Coulomb repulsion. At half filling, the ground state is the antiferromagnetic Néel state. Hole doping induces an electron deficiency which results into phase separation on the nanoscale. It is accommodated by locating the added holes in a periodic structure of microscopic lines. This spatial distribution minimizes the energy as compared to an homogeneous solution. The separation between hole stripes thus increases with decreasing doping until it diverges in the limit of half filling, and the charge modulation vanishes. One may then presume that another mechanism is necessary in order to stabilize a spin and charge modulation at exactly zero doping. However, finding such a phase in extensions of the model turned out unsuccessful^{23–31}. Hence, in an earlier study³², we introduced in this perspective a Hubbard Hamiltonian extended with a nearest-neighbor interaction term of amplitude V , as well as a checkerboard modulation $\pm\varepsilon$ of the energy levels which straightforwardly induces charge order in the antiferromagnetic phase. We then found that the model harbors charge order (CO) and joint spin and charge modulations (SCO) at finite values of the potential ε . The CO phase is realized by a staggering of compensating charge excess or charge depletion in both directions, and the SCO phase is realized by a staggering of compensated magnetic moments accompanying the above CO. The latter are reminiscent of stripes^{1,3–14,33–36} (for a review, see, *e.g.*, Ref. [2]), yet in the absence of hole doping.

The aim of the present paper is to deepen our understanding of the phases that have been unveiled in our previous paper, and that could be suitable for resistive switching. Indeed, we have determined that CO and SCO can coexist in parameter domains at the boundary between their respective regions of stability. The zero-temperature transition between the two phases is found to be first order, which could be harnessed for application in digital electronics. Indeed, resistive switching in Mott insulators currently drives a considerable research activity since the property could enable a variety of novel functions, such as energy-efficient data processing for artificial intelligence^{37–39}, resistive RAM for data storage^{40,41}, or optoelectronics^{42,43}. Furthermore, functional oxides also stand as promising replacements for conventional semiconductor materials when the latter will reach their intrinsic limitations at the nanoscale^{43,44}. V_2O_3 provides a prominent example^{45,46} but others are found among transition metal oxides such as VO_2 ^{47,48}, NbO_2 ^{49,50}, and Ca_2RuO_4 ^{51,52}.

This paper is organized as follows: In Sec. 2, the extended Hubbard model is presented, and the quasi-particle dispersion resulting from its treatment in the Kotliar and Ruckenstein slave-boson formalism is given. In Sec. 3, we perform a comparison of the band structure, of the charge order parameters, as well as of the spin-resolved renormalization factors between the charge ordered phase and the spin and charge ordered phase. We focus on the intermediate and stronger coupling regimes where resistive switching is most likely. Lastly, Sec. 4 concludes on these results and gives a brief outlook.

2 Model and methods

2.1 Extended Hubbard model

In our earlier study³², we extended the Hubbard model in two ways. First, an efficient screening of the long-range Coulomb interaction is assumed, which reduces the latter to local and nearest-neighbor couplings, only. Second, a staggered crystal field that may arise from

specific environments of the ions on which the interest is focused, is taken into account. For instance, in the context of LSCO superconductors, alternating La and, *e.g.*, Pr chains, could produce such a contribution to the crystal field, as the electronic cloud of the La cations is more extended than the one of the Pr cations. This results in a staggered 2ε energy distribution between adjacent lattice sites. One then arrives at the model Hamiltonian

$$\mathcal{H} = \mathcal{H}_0 + \mathcal{H}_\varepsilon + \mathcal{H}_U + \mathcal{H}_V. \quad (1)$$

Here the one-body part $\mathcal{H}_0 + \mathcal{H}_\varepsilon$, in the grand canonical ensemble, is made of

$$\mathcal{H}_0 = \sum_{i,j,\sigma} t_{ij} c_{i,\sigma}^\dagger c_{j,\sigma} - \mu \sum_{i,\sigma} c_{i,\sigma}^\dagger c_{i,\sigma}, \quad (2)$$

where $c_{i,\sigma}^\dagger$ ($c_{i,\sigma}$) creates (annihilates) an electron with spin $\sigma \in \{\uparrow, \downarrow\}$ at the lattice site i , t_{ij} is the hopping amplitude between lattice sites i and j , and μ is the chemical potential controlling the band filling. This is supplemented by a staggered local potential of the form

$$\mathcal{H}_\varepsilon = \sum_{i,\sigma} \varepsilon_i c_{i,\sigma}^\dagger c_{i,\sigma}, \quad (3)$$

with

$$\varepsilon_i = -\varepsilon \quad \text{if } i \in A, \quad (4a)$$

$$\varepsilon_i = +\varepsilon \quad \text{if } i \in B, \quad (4b)$$

where A and B are the two sublattices of a bipartite lattice. The next contribution is the local interaction term

$$\mathcal{H}_U = U \sum_i c_{i,\uparrow}^\dagger c_{i,\downarrow}^\dagger c_{i,\downarrow} c_{i,\uparrow}, \quad (5)$$

where U is the on-site Coulomb interaction strength. The last term models the intersite Coulomb interaction as

$$\mathcal{H}_V = \frac{1}{2} \sum_{\substack{\langle i,j \rangle \\ \sigma, \sigma'}} V_{ij} c_{i,\sigma}^\dagger c_{j,\sigma'}^\dagger c_{j,\sigma'} c_{i,\sigma}, \quad (6)$$

where V_{ij} is the coupling restricted to nearest-neighbor sites i and j . The $1/2$ factor accounts for the double-counting of the $\langle i, j \rangle \equiv \langle j, i \rangle$ pairs in the sum.

Throughout the present study, we consider hopping to nearest neighbors, only, and we work in the half-filled subspace of the square lattice, such that

$$\sum_{i,\sigma} \langle n_{i,\sigma} \rangle = N_L, \quad (7)$$

where $n_{i,\sigma}$ is the usual electron number operator ($n_i = n_{i,\uparrow} + n_{i,\downarrow}$), and N_L is the total number of lattice sites. We also set the lattice parameter $a = 1$ thereby fixing the length scale.

Parameter set	U/t	V/t	ε/t
I	4	0.5	0.1
II	4	1.2	0.1
III	8	1.8	0.1
IV	8	2.5	0.1

Table 1: Parameter sets used in Section 3.

2.2 The Kotliar and Ruckenstein representation

We treat the Hamiltonian in the Kotliar and Ruckenstein representation⁵³ on the saddle-point level of approximation. It is a well established approach, which has been tested in many ways^{54–61} (for key fundamental aspects see Refs. [62–67]), and applied to a series of problems in the thermodynamical limit^{54–57,59,68–73}. Here, we closely follow Ref. [32], and we stick to the notations and conventions used therein, up to one non-essential difference: instead of accounting for the staggered potential in the bosonic sector, we here do it in the fermionic one. Both calculations yield the same energy and boson expectation values, but the quasi-particle dispersion is modified into

$$E_{\mathbf{k},\sigma,\nu} = \bar{\beta}_\sigma - \mu + \nu \sqrt{(\tilde{z}_\sigma^2 t_{\mathbf{k}})^2 + (\Delta_\sigma^{SB} - \varepsilon)^2}, \quad \nu = \pm 1 \quad (8)$$

which reduces to the bare dispersion in the non-interacting limit, in contrast to Eq. (31) in Ref. [32].

3 Results

Following Ref. [32], we shall mainly present results for two representative values of ε in this study, namely $\varepsilon = 0.1 t$ and $\varepsilon = t$, as the proposed nature of the staggered local potential does not suggest large values for ε . Moreover, we focus on the case of a half-filled band. In our earlier work, one of the main results was that, for finite ε , the CO and SCO phases coexist in large regions of the (U, V) parameter space, but little detail was provided regarding the nature of this coexistence. Evidence was also given that the properties of the phases qualitatively differ in the intermediate coupling regime from the strong coupling regime.

In the limit $t \rightarrow 0$, the study of our model considerably simplifies and we are left with two potential ground states: (i) a pair density wave of energy per site $U/2 - \varepsilon$, and (ii) an homogeneous state with one electron per site, of energy per site $2V$. Both are degenerate for $U = 4V + 2\varepsilon$ and one expects a finite hopping to modify this phase boundary, and even to transform the associated phase transition into a continuous one. Yet, according to Ref. [32], this does not happen, but the phase transition remains close to the $U = 4V + 2\varepsilon$ line. Also, a great deal of information arises from the quasiparticle dispersion and order parameters, on which this study focuses. They are presented in this section, for four representative parameter sets, given in Table 1.

3.1 Intermediate coupling

According to the above, we focus the first part of our study on the intermediate coupling value of $U = 4t$, and address the parameter sets I and II, which are located on both sides of

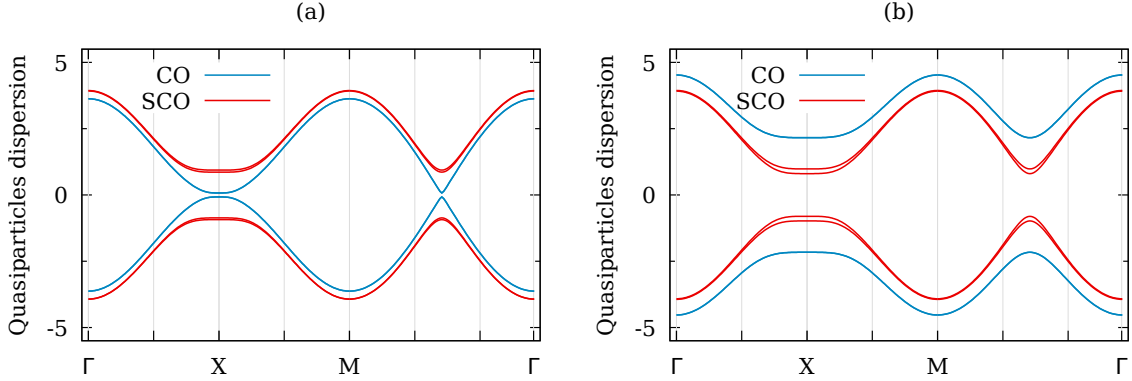


Figure 1: Band structure of the CO and SCO phases at $U = 4t$, $\varepsilon = 0.1t$ and $V = 0.5t$ (a), and $V = 1.2t$ (b).

the $U = 4V + 2\varepsilon$ line. In this section, we thus present our results concerning the properties of both phases for these two parameter sets.

Fig. 1(a) displays the quasiparticle dispersion in both phases for the parameter set I. In this case, the SCO phase is the ground state while the CO phase is metastable. We notice that the CO phase is only weakly gapped, with a gap of about $0.14t$. This, as argued below, hints at the existence of a parameter range, surrounding the present one, in which pure charge ordered solutions displaying modest charge modulations may be found. In this case, the couplings are too weak to induce sizable charge modulations in the phase. As for the SCO phase, it remains gapped in this region, with a gap of about $1.87t/1.72t$ for each spin branch, respectively. For these parameter values, the antiferromagnetic ordering of the SCO phase dominates, which leads to a band structure qualitatively similar to that of the pure spin-density waves of the t - U - V model. We begin to discern, however, the peculiar four-band structure characteristic of the SCO phase, but the fact that these bands remain pairwise nearly degenerate implies that, aside from an expected modest charge modulation, the charge distribution should still appear as predominantly homogeneous for these parameter values. Besides, we find the two independent subbands of the SCO phase to be $3.00t/3.06t$ wide, while the width of the subband of the CO phase is $3.55t$. They are hence narrower in the former case, as expected from the larger gap.

In Fig. 1(b), we show the impact of an increase in V on the band structure of both phases. We take $V = 1.2t$ as a representative value, that is, for the parameter set II. In this case, the ground state is now the CO phase, with the SCO phase being metastable. We further see that the gap open in the CO phase considerably increased from $0.14t$ to about $5t$, which suggests a more firmly established charge order. Besides, the quasiparticle dispersion of the SCO phase did not qualitatively evolve from the previous case, the only noticeable modification being that the difference in the respective gaps of both spin-projection branches of the dispersion has now increased to $1.61t$ and $1.96t$. This could be interpreted as the influence of a more pronounced charge order in the SCO phase, due to the larger value of V , which increasingly lifts the degeneracy between the bands. The subband width also changed from $3.00t/3.06t$ to $2.96t/3.11t$.

The saddle-point values of the physical quantities of interest are shown in Fig. 2 as func-

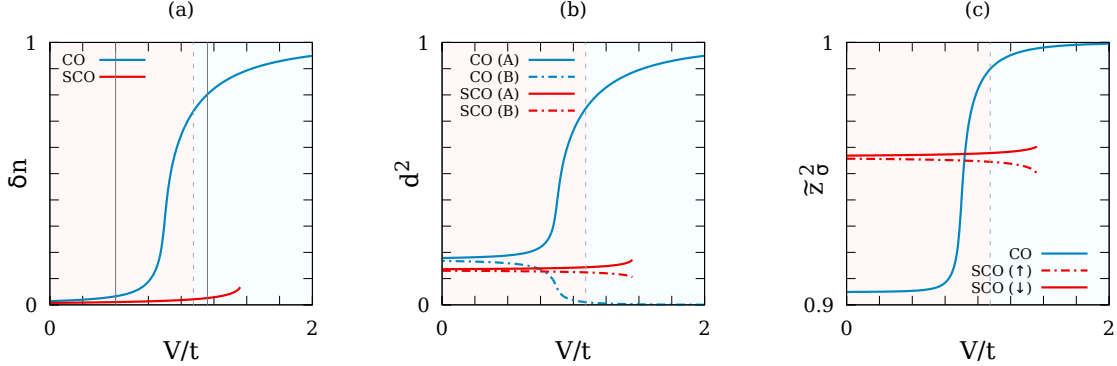


Figure 2: Charge modulation (a), sublattice resolved double occupancy (b), and spin resolved renormalization factor (c) of the CO and SCO phases for $U = 4 t$ and $\varepsilon = 0.1 t$ as functions of V . The dashed gray line denotes the SCO-CO phase transition. The solid gray lines denote the parameter sets I and II.

tions of V , for fixed $U = 4 t$ and $\varepsilon = 0.1 t$. They involve the charge modulation

$$\delta n = (n_A - n_B)/2, \quad (9)$$

the sublattice resolved double occupancy

$$d_{A/B}^2 = \langle d^2 \rangle \pm \delta d^2, \quad (10)$$

and the spin resolved renormalization factors

$$\tilde{z}_\sigma^2 = z_{A,\sigma} z_{B,\sigma}, \quad (11)$$

where we introduced the sublattice and spin resolved Gutzwiller factors $z_{A/B,\sigma}$ (see, e.g., Eq. (34b) in Ref. [32]). As can be seen from Fig. 2(a) and Fig. 2(b), for small values of the intersite coupling ($V \lesssim 0.5 t$), the charge order is only weakly established, even in the CO phase, as the values of δn and δd^2 are smaller than 10^{-2} . This owes to the fact that the relevant energy scale for such small values of V is the on-site coupling U , favoring the antiferromagnetic arrangement of the spins with no charge modulation at half-filling. When increasing V , one notices a slight increase in the charge ordering of the SCO phase, with δn eventually going from 7.39×10^{-3} for $V = 0$ to 6.72×10^{-2} for $V = 1.45 t$ (δd^2 takes similar values in this range of V). Beyond this value of V , the SCO solutions to the saddle-point equations (SPE) vanish and only CO solutions remain. We thus refer to the line in (U, V) space at which the SCO solutions vanish as the SCO end-line. Conversely, the CO solutions remain stable for every shown values of V , leading to a nearly fully-established charge order for $V = 2 t$, with values of δn and δd^2 close to 0.95. For this moderate V , yet fulfilling $V > U/4 - \varepsilon/2$, we thus meet a phase which strongly resembles a pair density wave, with one sublattice being nearly fully doubly-occupied, while the other sublattice remains essentially empty.

These order parameters also help to qualitatively understand the phase diagram. When the ground state is the SCO phase, for low values of V , the $-4V\delta n^2$ contribution to the

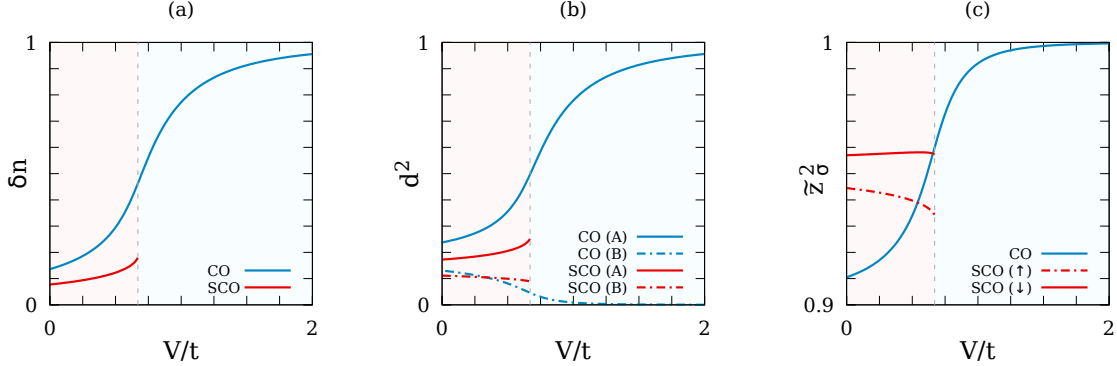


Figure 3: Charge modulation (a), sublattice resolved double occupancy (b), and spin resolved renormalization factor (c) of the CO and SCO phases for $U = 4t$ and $\varepsilon = t$ as functions of V . The dashed grey line denotes the SCO-CO phase transition.

free energy is irrelevant in both phases, and their respective free energies essentially differ via the term $U\langle d^2 \rangle$. Since the CO phase has the largest value of $\langle d^2 \rangle$, it naturally has a larger energy, leading to the SCO ground state. At larger values of V , however, the $-4V\delta n^2$ becomes predominant and, as δn is an order of magnitude larger in the CO phase than in the SCO one, the ground state thus becomes CO.

Regarding the renormalization factors, which are displayed in Fig. 2(c), one can see that it is minimal in the CO phase for small values of V — with a value of about 0.95. It however harbors a sharp increase for values of V ranging from $0.75t$ to t , corresponding to the value at which the charge order begins to sharply increase in the CO phase as well. This indicates that the charge modulations tend to hinder the correlations originating from the on-site interactions, as they are produced for smaller values of the ratio U/V . In the SCO phase, however, the renormalization factors for the up and down spin branches of the dispersion remain very close to one another for small values of V , with values averaging to 0.98 and a relative difference of roughly 3×10^{-4} for $V = 0$. This relative difference slightly increases as V is increased, but remains small as it only reaches approximately 3×10^{-3} at the SCO end point.

In Fig. 3, the same quantities as in Fig. 2 are shown, again as functions of V and for fixed $U = 4t$ but we now increase the staggered potential to $\varepsilon = t$. We notice from Fig. 3(a) and Fig. 3(b) that the charge order is now more pronounced, even at $V = 0$, confirming that larger values of ε tend to increase the charge modulations even when U is the dominant energy scale. For these values of U and ε , the SCO-CO transition line corresponds to the SCO end-line, since in this regime, the SCO solutions to the SPEs vanish while still being lower in energy than the CO solutions. In the SCO phase, we again see that the charge modulations become increasingly pronounced as V is increased towards the SCO end-point, with δn ranging from 0.08 to 0.18 for V between 0 and $0.67t$, and δd^2 ranging from 0.03 to 0.08 in the same V -interval. The stronger dependence of these quantities on V as compared to the $\varepsilon = 0.1t$ case implies that the effect of the intersite coupling is enhanced by the larger residual charge order caused by ε at $V = 0$. Besides, in the CO phase, the situation is qualitatively similar to the $\varepsilon = 0.1t$ case for large values of V . The main difference lies in the $V \lesssim 0.75t$ range, in which

the minimal charge order imposed by $\varepsilon = t$ causes the CO solutions to be more sensitive to variations in V .

Regarding the renormalization factors in Fig. 3(c), we see that the relative difference between both spin branches of the dispersion in the SCO phase has increased, with $\tilde{z}_\sigma \sim 0.975 \pm 0.003$ for $V = 0$ and $\tilde{z}_\sigma \sim 0.972 \pm 0.006$ for $V = 0.67 t$. As argued above, this owes to the stronger charge order in the SCO phase at $\varepsilon = t$, as compared to the $\varepsilon = 0.1 t$ case. For the CO phase, the renormalization factor takes the value 0.91 for $V = 0$, indicating a slight increase in the effect of the local correlations as compared to the previous case. Similarly to its $\varepsilon = 0.1 t$ counterpart, the renormalization factor increases with V , up to $\tilde{z}_\sigma = 1$, but with a smaller slope in this case — suggesting a smoother transition from the residual charge ordered regime to the V -driven one.

Comparison of the interplay of the SCO and CO phases between the two presented values of ε thus showed that, on one hand, the nature of the SCO and CO phases remain qualitatively independent on ε when it is smaller than the U and V couplings. On the other hand, the charge order at low values of the intersite coupling seems to be strongly driven by ε in both phases, with larger values of ε implying not only stronger charge modulations, but an enhanced V -dependence of the charge order as well. Additionally, we emphasize that all these quantities are subject to a discontinuous variation at the SCO-CO transition, which occurs when the free energy of both phases become degenerate for $\varepsilon = 0.1 t$ and when the SCO solutions vanish for $\varepsilon = t$. This thus confirms the first-order character of the phase transition between these two phases.

3.2 Stronger coupling

In the stronger coupling regime where U is larger than the bandwidth, here $U = 8 t$, the energy scales of the interactions U and V prevail over the amplitude of the staggered local potential. In this way, one would expect to recover, at least qualitatively, the behavior of the well studied t - U - V model at half-filling^{29–31}, in which a spin-density wave and a charge-density wave compete at zero temperature, with a phase transition at $V = U/4$. In our study, the CO phase would then be the analog of the charge-density wave, albeit not spontaneously formed due to the finite value taken by ε , and the SCO phase would be the analog of the spin-density wave favored by the local interaction U .

Fig. 4(a) displays the band structure of both phases for the parameter set III. In this case, the SCO phase is the ground state. One can see that both phases are strongly gapped in this regime, with a gap of about $4.6 t$ in the CO phase and $6 t$ in the SCO phase. Additionally, Fig. 4(b) presents the band structure of both phases for the parameter set IV, in which V is increased to $2.5 t$. This corresponds to a region of the phase diagram in which the CO phase is the ground state, while the SCO phase is metastable. Compared to Fig. 4(a), the gap of the CO phase increased more than twofold, reaching a value of about $11.2 t$. This implies that the charge order is much more firmly established in the CO phase for $V = 2.5 t$ than it is for $V = 1.8 t$. As for the SCO phase, one can see that its band structure has barely evolved after the increase in V . Moreover, no noticeable lifting of the pairwise degeneracy of the bands in this phase is observed. This hints at the fact that, in this regime, the SCO phase remains qualitatively independent on the value of V and is essentially a slightly deformed version of the pure spin-density wave of the t - U - V model.

In order to verify these interpretations, let us now turn to the saddle-point values of the

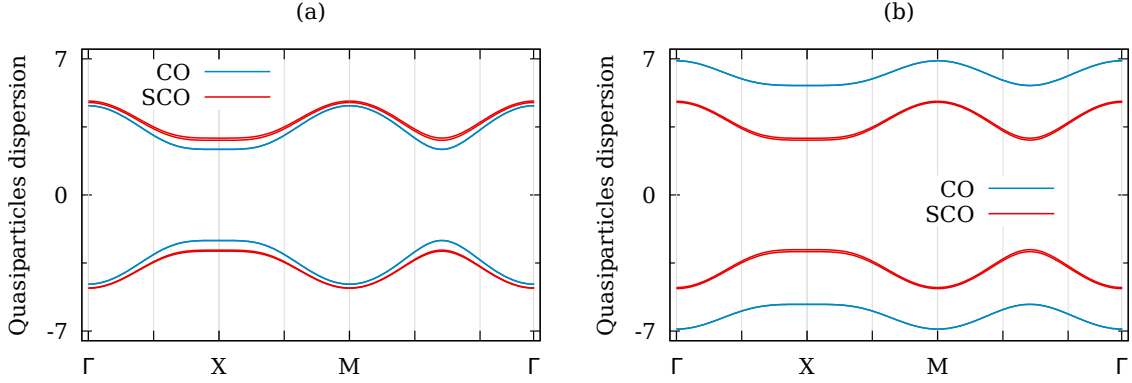


Figure 4: Band structure of the CO and SCO phases at $U = 8 t$, $\varepsilon = 0.1 t$ and $V = 1.8 t$ (a), and $V = 2.5 t$ (b).

quantities of interest in this stronger coupling regime. The charge modulation, the double occupancy and the renormalization factors for the parameter set $U = 8 t$ and $\varepsilon = 0.1 t$ are displayed in Fig. 5, in dependence on V . One can see from Fig. 5(a) and Fig. 5(b) that the charge modulation in the SCO phase are barely noticeable, reaching, at most, 3.8×10^{-3} for $V = 3 t$. Likewise, the double occupancy is very weakly modulated as we find it to be $(5.56 \pm 0.17) \times 10^{-2}$ for $V = 3 t$. This implies that, in this regime, the charge distribution in the SCO phase is nearly homogeneous, and it is only the spin modulation that remains sizable (see Fig. 4 in³²). As for the CO phase, we note the appearance of a CO end-line, below which the purely charge ordered solutions cease to exist. Above this end-line, the charge modulation of the CO phase strongly depends on V , with δn and δd^2 displaying a nearly vertical slope above $V = 1.67 t$, at which $\delta n \sim 0.675$ and $d_{A,B}^2 \sim 0.35 \pm 0.34$. Then, at large V , δn approaches 1 while $d_{A,B}^2$ approaches 0.5 ± 0.5 , implying that the pair-density wave is almost fully established.

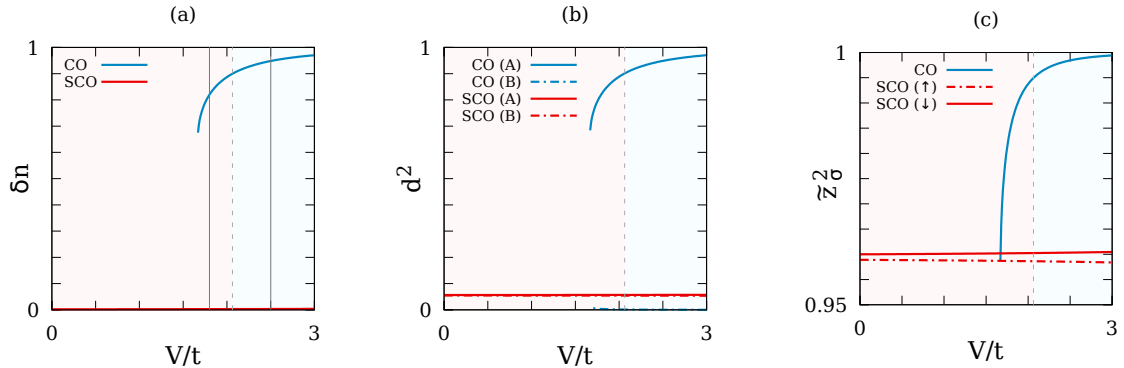


Figure 5: Charge modulation (a), sublattice resolved double occupancy (b), and spin resolved renormalization factor (c) of the CO and SCO phases for $U = 8 t$ and $\varepsilon = 0.1 t$ as functions of V . The dashed gray line denotes the SCO-CO phase transition. The solid gray lines denote the parameter sets III and IV.

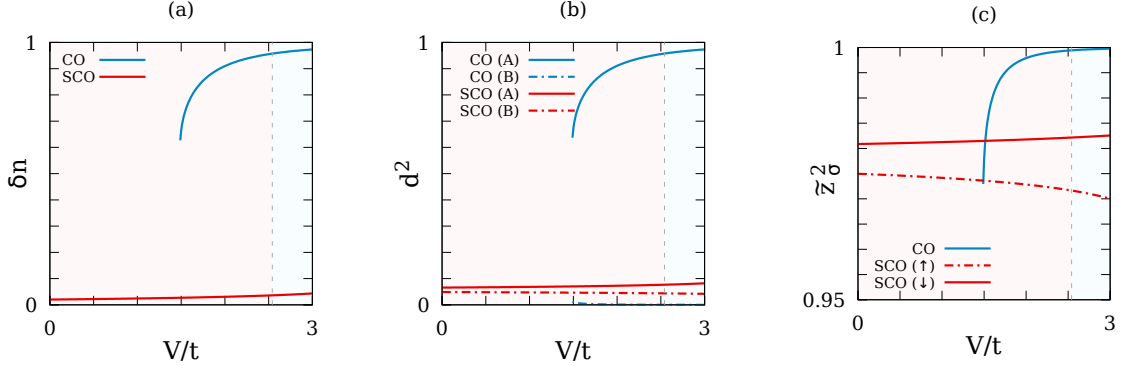


Figure 6: Charge modulation (a), sublattice resolved double occupancy (b), and spin resolved renormalization factor (c) of the CO and SCO phases for $U = 8t$ and $\varepsilon = t$ as functions of V . The dashed grey line denotes the SCO-CO phase transition.

One can infer, from the renormalization factors in Fig. 5(c), that the situation is qualitatively similar to that of the intermediate coupling case discussed above. Indeed, the renormalization factors of the SCO phase show very weak dependence on V , taking values of about 0.958 for $V = 0$ and increasing (or decreasing) by less than 3% when V is increased to $3t$. Such a weak V -dependence of \tilde{z}_σ owes to the fact that, in this coupling regime, the SCO phase is largely dominated by its spin modulations, while the charges remain nearly homogeneously distributed, irrespective of the value of V . In contrast, in the CO phase, the renormalization factor takes the value 0.958 at the end-point $V = 1.67t$, and sharply increases with V , saturating to 1 for large values of V . This again indicates that, in the large- V CO phase, the static correlations induced by local interactions at half-filling are mostly suppressed when a genuine pair-density wave sets in.

In Fig. 6, the same quantities are presented, as functions of V , for $U = 8t$ and for an increased $\varepsilon = t$. As in the intermediate coupling case, we notice that the increase in ε induces an enhanced charge ordering in both phases. Specifically, one can see in Fig. 6(a) and Fig. 6(b) that the charge order in the SCO phase becomes noticeably V -dependent, with δn ranging from 2.02×10^{-2} to 4.34×10^{-2} , as well as $d_{A,B}^2$ ranging from $(5.7 \pm 0.8) \times 10^{-2}$ to $(6.2 \pm 2.0) \times 10^{-2}$, for V between 0 and $3t$. In the CO phase, the situation is qualitatively similar to the $\varepsilon = 0.1t$ case, with an end-point at $V = 1.49t$, below which no CO solutions to the SPE exist. At this end-point, we find $\delta n \sim 0.63$ and $d_{A,B}^2 \sim 0.32 \pm 0.31$, followed by a sharp increase towards the pair-density wave limit with $\delta n = 1$ and $d_{A,B}^2 = 0.5 \pm 0.5$ when increasing V .

Fig. 6(c) shows that, as in the intermediate coupling case, the increase in the staggered potential enhances the difference in the renormalization factors of the SCO phase, with $\tilde{z}_\sigma^2 \sim 0.956 \pm 0.006$ for $V = 0$ and $\tilde{z}_\sigma^2 \sim 0.953 \pm 0.012$ for $V = 3t$. In terms of absolute values, these renormalization factors are a few percents lower than their $\varepsilon = 0.1t$ counterpart. This is further evidence that the charge order induced by ε and V in the SCO phase hinders the effect of local correlations, as, e. g., for $\varepsilon = V = 0$ (pure spin-density wave) we find that \tilde{z}_σ^2 takes the value 0.905 for $U = 4t$, and 0.619 for $U = 8t$. As for the CO phase, the tendencies are again the same as in the $\varepsilon = 0.1t$ case, namely a sharp increase from the end-point

$V = 1.49 t$, going from $\tilde{z}_\sigma^2 \sim 0.947$ to $\tilde{z}_\sigma^2 = 1$ at large V , when the pair-density wave becomes fully established.

In this stronger coupling regime, we have thus unraveled that the picture becomes simpler than at intermediate coupling. Indeed, on one hand, the SCO phase essentially reduces to its antiferromagnetic spin modulations, with small inhomogeneities in its charge distribution for sufficiently large values of ε and V . On the other hand, the CO phase, for values of the parameters for which it exists, strongly resembles a genuine pair-density wave, in which one sublattice is totally filled while the remaining one is essentially empty.

Lastly, let us briefly discuss the strong coupling regime. When one of the energy scale becomes arbitrarily large, the picture simplifies even more. Specifically, if U is much larger than the bare bandwidth, while V and ε remain smaller than the latter, the SCO phase loses its dependence on V and ε , and a phase strongly resembling the genuine spin-density wave, with energy close to $2V$, is found. As for the CO phase, it is simply not stabilized in this regime. Conversely, if V or ε become arbitrarily large as compared to the bare bandwidth, while U remains smaller than the latter, we find that no SCO solutions exist anymore, whereas the CO phase becomes the genuine pair-density wave, with energy $U/2 - \varepsilon$.

4 Discussion and summary

Summarizing, we presented above the quasiparticle dispersions and the order parameters characterizing the two phases that coexist in the half-filled ε - t - U - V extended Hubbard model when tackled in the Kotliar and Ruckenstein slave-boson representation. For $U \lesssim 4V + 2\varepsilon$, the ground state is charge ordered. In that case, we obtain the renormalization factors \tilde{z}_σ to modestly differ from one. This also remains true in the regions of the phase diagram in which the ground state is spin-and-charge ordered. Accordingly, we find it useful to use the Hartree-Fock approximation expressions of the gaps, since they are easier to interpret than their Kotliar and Ruckenstein slave-boson counterpart. Following Ref. [32], they read $\Delta_\sigma^{HF} = |(8V - U)\delta n + \sigma U m_z + 2\varepsilon|$, with $\sigma = \pm 1$ and m_z the staggered magnetization. They highlight the complex origin of the gaps and their sophisticated dependence on the parameters of the model. In the non-interacting limit, the two gaps collapse into a single one given by $2|\varepsilon|$. It therefore has a charge character, which unravels the physics embedded in the crystal field. This charge character of the gap is manifest in the limit of vanishing U and ε , too, as well as when U is the only vanishing parameter. In this latter case, the gap never closes. Indeed, positive ε pins the charge density wave to have its maxima on the A sites, rendering δn positive. Hence the gap remains open for $V > 0$. For $V < 0$, with $4|V| \gg \varepsilon$, the charge distribution remains largely homogeneous, so that $|4V\delta n| < \varepsilon$ and no gap closing takes place. The case $\varepsilon < 0$ may be discussed in the very same fashion, after having exchanged the A and B sublattices. Conversely, when U is the only non-vanishing parameter, both gaps merge into a single one, which now has a magnetic character. Hence, at last, the two gaps that open in the SCO phase arise from their joint charge and magnetic characters.

Quantitatively, the above Hartree-Fock expressions nicely explain the evolution of the gaps found when performing the calculations with the parameter sets I–IV, which dictate the behavior of the above discussed subband widths. This follows from the finding that the spin-resolved renormalization factors \tilde{z}_σ remain close to one in the entire phase coexistence region of the phase diagram.

Also, it is worth noticing that the physics of joint spin and charge modulations in the SCO phase is enabled by a finite, but not necessarily sizable, value of ε . The ensuing interplay between the CO and SCO phases is thus relevant even when ε is orders of magnitude smaller than the energy scale of the interactions, as is shown by the results for $\varepsilon = 0.1 t$ at intermediate and stronger coupling.

Lastly, let us emphasize that these large regions of phase coexistence between two insulating phases harboring quantitatively distinct gaps shows great potential in the tailoring of materials prone to resistive switching.

Acknowledgments

This work was supported by Région Normandie through the ECOH project.

References

- [1] J. Tranquada, B. Sternlieb, J. Axe, Y. Nakamura, and S. Uchida, *Nature* **375**, 561 (1995).
- [2] J. M. Tranquada, *Adv. Phys.* **69**, 437 (2020).
- [3] L. Wu, Y. Shen, A. M. Barbour, W. Wang, D. Prabhakaran, A. T. Boothroyd, C. Mazzoli, J. M. Tranquada, M. P. M. Dean, and I. K. Robinson, *Phys. Rev. Lett.* **127**, 275301 (2021).
- [4] G. Campi, A. Bianconi, B. Joseph, S. K. Mishra, L. Müller, A. Zozulya, A. A. Nugroho, S. Roy, M. Sprung, and A. Ricci, *Sci. Rep.* **12**, 2045 (2022).
- [5] J. M. Tranquada, D. J. Buttrey, V. Sachan, and J. E. Lorenzo, *Phys. Rev. Lett.* **73**, 1003 (1994).
- [6] V. Sachan, D. J. Buttrey, J. M. Tranquada, J. E. Lorenzo, and G. Shirane, *Phys. Rev. B* **51**, 12742 (1995).
- [7] M. Cwik, M. Benomar, T. Finger, Y. Sidis, D. Senff, M. Reuther, T. Lorenz, and M. Braden, *Phys. Rev. Lett.* **102**, 057201 (2009).
- [8] H. Ulbrich and M. Braden, *Physica C: Superconductivity* **481**, 31 (2012).
- [9] S.-W. Cheong, H. Y. Hwang, C. H. Chen, B. Batlogg, L. W. Rupp, and S. A. Carter, *Phys. Rev. B* **49**, 7088 (1994).
- [10] M. Hücker, M. von Zimmermann, and G. D. Gu, *Phys. Rev. B* **75**, 041103(R) (2007).
- [11] M. Hücker, M. v. Zimmermann, G. D. Gu, Z. J. Xu, J. S. Wen, G. Xu, H. J. Kang, A. Zheludev, and J. M. Tranquada, *Phys. Rev. B* **83**, 104506 (2011).
- [12] M. Raczkowski, R. Frésard, and A. M. Oleś, *Phys. Rev. B* **73**, 174525 (2006).
- [13] A. Himeda, T. Kato, and M. Ogata, *Phys. Rev. Lett.* **88**, 117001 (2002).

- [14] K. Ido, T. Ohgoe, and M. Imada, Phys. Rev. B **97**, 045138 (2018).
- [15] S. R. White and D. J. Scalapino, Phys. Rev. B **79**, 220504 (2009).
- [16] T. Huang, C. Mendl, H. Jiang, B. Moritz, and T. Devereaux, NPJ Quantum Materials **3**, 22 (2018).
- [17] P. Corboz, T. M. Rice, and M. Troyer, Phys. Rev. Lett. **113**, 046402 (2014).
- [18] B. Ponsioen, S. S. Chung, and P. Corboz, Phys. Rev. B **100**, 195141 (2019).
- [19] J.-W. Li, B. Bruognolo, A. Weichselbaum, and J. von Delft, Phys. Rev. B **103**, 075127 (2021).
- [20] A. Leprévost, O. Juillet, and R. Frésard, New J. Phys. **17**, 103023 (2015).
- [21] Y.-F. Jiang, J. Zaanen, T. P. Devereaux, and H.-C. Jiang, Phys. Rev. Research **2**, 033073 (2020).
- [22] B.-X. Zheng, C.-M. Chung, P. Corboz, G. Ehlers, M.-P. Qin, R. M. Noack, H. Shi, S. R. White, S. Zhang, and G. K.-L. Chan, Science **358**, 1155 (2017).
- [23] P. G. J. van Dongen, Phys. Rev. B **49**, 7904 (1994).
- [24] P. G. J. van Dongen, Phys. Rev. B **50**, 14016 (1994).
- [25] U. Wolff, Nucl. Phys. B **225**, 391 (1983).
- [26] M. Deeg, H. Fehske, and H. Büttner, Z. Phys. B **91** (1993).
- [27] J. E. Hirsch, Phys. Rev. Lett. **53**, 2327 (1984).
- [28] P. Sengupta, A. W. Sandvik, and D. K. Campbell, Phys. Rev. B **65**, 155113 (2002).
- [29] Y. Zhang and J. Callaway, Phys. Rev. B **39**, 9397 (1989).
- [30] H. Terletska, T. Chen, and E. Gull, Phys. Rev. B **95**, 115149 (2017).
- [31] J. Paki, H. Terletska, S. Isakov, and E. Gull, Phys. Rev. B **99**, 245146 (2019).
- [32] L. Philoxene, V. H. Dao, and R. Frésard, Phys. Rev. B **106**, 235131 (2022).
- [33] S. Yamamoto, T. Fujiwara, and Y. Hatsugai, Phys. Rev. B **76**, 165114 (2007).
- [34] U. Schwingenschlögl, C. Schuster, and R. Frésard, EPL **81**, 27002 (2008).
- [35] U. Schwingenschlögl, C. Schuster, and R. Frésard, EPL **88**, 67008 (2009).
- [36] M. Raczkowski, R. Frésard, and A. M. Oleś, Phys. Rev. B **73**, 094429 (2006).
- [37] J. Del Valle, J. G. Ramírez, M. J. Rozenberg, and I. K. Schuller, J. Appl. Phys. **124**, 211101 (2018).
- [38] J. Del Valle, P. Salev, F. Tesler, N. M. Vargas, Y. Kalcheim, P. Wang, J. Trastoy, M.-H. Lee, G. Kassabian, J. G. Ramírez, *et al.*, Nature **569**, 388 (2019).

- [39] S. R. Bauers, M. B. Tellekamp, D. M. Roberts, B. Hammett, S. Lany, A. J. Ferguson, A. Zakutayev, and S. U. Nanayakkara, *Nanotechnology* **32**, 372001 (2021).
- [40] E. Janod, J. Tranchant, B. Corraze, M. Querré, P. Stoliar, M. Rozenberg, T. Cren, D. Roditchev, V. T. Phuoc, M.-P. Besland, *et al.*, *Adv. Funct. Materials* **25**, 6287 (2015).
- [41] Y. Wang, K.-M. Kang, M. Kim, H.-S. Lee, R. Waser, D. Wouters, R. Dittmann, J. J. Yang, and H.-H. Park, *Materials Today* **28**, 63 (2019).
- [42] Z. Liao, N. Gauquelin, R. J. Green, K. Müller-Caspary, I. Lobato, L. Li, S. Van Aert, J. Verbeeck, M. Huijben, M. N. Grisolia, *et al.*, *Proc. Natl. Acad. Sci. USA* **115**, 9515 (2018).
- [43] M. Coll, J. Fontcuberta, M. Althammer, M. Bibes, H. Boschker, A. Calleja, G. Cheng, M. Cuoco, R. Dittmann, B. Dkhil, *et al.*, *Appl. Surf. Sci.* **482**, 1 (2019).
- [44] H. Takagi and H. Y. Hwang, *Science* **327**, 1601 (2010).
- [45] F. A. Chudnovskii, A. L. Pergament, G. B. Stefanovich, P. A. Metcalf, and J. M. Honig, *J. Appl. Phys.* **84**, 2643 (1998).
- [46] J. S. Brockman, L. Gao, B. Hughes, C. T. Rettner, M. G. Samant, K. P. Roche, and S. S. P. Parkin, *Nature Nanotech.* **9**, 453 (2014).
- [47] T. Driscoll, H.-T. Kim, B.-G. Chae, M. Di Ventra, and D. N. Basov, *Appl. Phys. Lett.* **95**, 043503 (2009).
- [48] J. Kim, C. Ko, A. Frenzel, S. Ramanathan, and J. E. Hoffman, *Appl. Phys. Lett.* **96**, 213106 (2010).
- [49] X. Liu, S. Md Sadaf, M. Son, J. Shin, J. Park, J. Lee, S. Park, and H. Hwang, *Nanotech.* **22**, 475702 (2011).
- [50] S. Kumar, J. P. Strachan, and R. Stanley Williams, *Nature* **548**, 318 (2017).
- [51] F. Nakamura, M. Sakaki, Y. Yamanaka, S. Tamaru, T. Suzuki, and Y. Maeno, *Sci. Rep.* **3**, 2536 (2013).
- [52] F. Pan, S. Gao, C. Chen, C. Song, and F. Zeng, *Mater. Sci. Eng. R Rep.* **83**, 1 (2014).
- [53] G. Kotliar and A. E. Ruckenstein, *Phys. Rev. Lett.* **57**, 1362 (1986).
- [54] L. Lilly, A. Muramatsu, and W. Hanke, *Phys. Rev. Lett.* **65**, 1379 (1990).
- [55] R. Frésard, M. Dzierzawa, and P. Wölfle, *Europhys. Lett.* **15**, 325 (1991).
- [56] R. Frésard and K. Doll, “The Hubbard Model: Its Physics and Mathematical Physics,” (NATO ARW, 1995) p. 385.
- [57] W. Zimmermann, R. Frésard, and P. Wölfle, *Phys. Rev. B* **56**, 10097 (1997).
- [58] V. H. Dao and R. Frésard, *Phys. Rev. B* **95**, 165127 (2017).

- [59] D. Riegler, M. Klett, T. Neupert, R. Thomale, and P. Wölfle, *Phys. Rev. B* **101**, 235137 (2020).
- [60] R. Frésard and P. Wölfle, *J. Phys.: Condens. Matter* **4**, 3625 (1992).
- [61] K. Steffen, R. Frésard, and T. Kopp, *Phys. Rev. B* **95**, 035143 (2017).
- [62] R. Frésard and P. Wölfle, *Int. J. Mod. Phys. B* **06**, 685 (1992).
- [63] S. Florens, A. Georges, G. Kotliar, and O. Parcollet, *Phys. Rev. B* **66**, 205102 (2002).
- [64] R. Frésard and T. Kopp, *Nucl. Phys. B* **594**, 769 (2001).
- [65] R. Frésard, H. Ouerdane, and T. Kopp, *Nucl. Phys. B* **785**, 286 (2007).
- [66] R. Frésard and T. Kopp, *Ann. Phys. (Berlin)* **524**, 175 (2012).
- [67] V. H. Dao and R. Frésard, *Ann. Phys. (Berlin)* **532**, 1900491 (2020).
- [68] P. A. Igoshev, M. A. Timirgazin, V. F. Gilmutdinov, A. K. Arzhnikov, and V. Y. Irkhin, *J. Phys.: Condens. Matter* **27**, 446002 (2015).
- [69] P. A. Igoshev and V. Y. Irkhin, *Phys. Rev. B* **104**, 045109 (2021).
- [70] M. Raczkowski, R. Frésard, and A. M. Oleś, *Europhys. Lett.* **76**, 128 (2006).
- [71] G. Seibold, E. Sigmund, and V. Hizhnyakov, *Phys. Rev. B* **57**, 6937 (1998).
- [72] R. Frésard and M. Lambole, *J. Low Temp. Phys.* **126**, 1091 (2002).
- [73] R. Frésard, K. Steffen, and T. Kopp, *Phys. Rev. B* **105**, 245118 (2022).